Time-Division ISAC Enabled Connected Automated Vehicles Cooperation Algorithm Design and Performance Evaluation

Qixun Zhang, *Member, IEEE*, Hongzhuo Sun, *Member, IEEE*, Xinye Gao, *Graduate Student Member, IEEE*, Xinna Wang, *Member, IEEE*, and Zhiyong Feng, *Senior Member, IEEE*

***Abstract*— To overcome the bottleneck of unreliable environment sensing caused by sensor failure and obstacle blockage, the cooperation among connected automated vehicles (CAVs) is crucial for the reliable and efficient raw sensing data sharing in order to guarantee the driving safety. Empowered by the narrow beamwidth and high data rate abilities, the millimeter wave (mmWave) communication technology can substantially improve the environment sensing ability among multiple CAVs. In this paper, a mmWave enabled CAVs cooperation algorithm is designed based on the proposed time-division integrated sensing and communication (TD-ISAC) system for raw sensing data sharing among CAVs. Considering various computing abilities at vehicle and infrastructure, a closed-form solution to the V2V or V2V/V2I cooperative communication mode selection is theoretically achieved based on response delay analysis to guarantee the timeliness of raw sensing data sharing. And the age of information based system status update algorithm is proposed for the V2V/V2I collaborative communication mode. The feasibility of the proposed TD-ISAC system is verified by simulation and hardware testbed results. Based on simulation results, the proposed communication mode selection algorithm can effectively minimize the response time delay in different conditions. The mmWave enabled TD-ISAC hardware testbed is developed and the position error of target detection can be reduced by 18.5 % using the sensing data fusion from two vehicles, while the communication throughput remains over 2.2 Gbps.**

***Index Terms*— Integrated sensing and communication, connected automated vehicles, age of information.**

I. Introduction

With the rapid development of 5G mobile communication system and artificial intelligence technology, the autonomous driving vehicles (ADVs) are developing fast which will change the life style of how people commute on the road. The environment sensing ability of a single ADV can be improved using multiple sensors on-board [1], such as the ultrasonic sensors, light detection and ranging (LiDAR), optical cameras, millimeter wave (mmWave) radars and so on. However, the performance of sensors is vulnerable to the light intensity, rain, obstacle in a hostile environment for ADVs. The idea of ADVs cooperation by using wideband wireless communication technology can enhance the sensing ability of a single ADV and improve the driving safety. But, different types of sensors will generate a great amount of raw sensing data over Gbps according to [2], leading to the efficient and robust data sharing among ADVs as a big challenge.

Therefore, ADVs enabled by 5G mmWave communication technology seems to be a promising solution to tackle the aforementioned challenge [3]. Vehicles equipped with in-vehicle sensors and vehicle-to-everything (V2X) communication equipment to support autonomous driving applications are defined as connected automated vehicles (CAVs) by ITU-R standard [4]. With the help of 5G communication technology, the transmission of raw sensing data among CAVs can be realized to support the multi-vehicle cooperative autonomous driving [5], [6]. But, in terms of the limited spectrum resources for V2X technology, the idea of integrated sensing and communication (ISAC) using the same frequency band has the potential to reduce the latency of information transfer among different types of communication and sensing systems, and improve the spectrum utilization efficiency.

Recently, the research works on ISAC system have attracted much interest by the efficient sensing data sharing among vehicles to enhance the performance and safety of autonomous driving [7]. Many technologies to realize ISAC functions have been proposed, such as using radar detection information to assist the mmWave communication [8]–[12], embedding communication data in radar signals to design integrated waveforms [13], and using IEEE 802.11ad standard to design radar waveforms [14]. Besides, the accurate channel estimation is made by using communication receiver to decode the radar frequency-hopping signals [15]. The performance indicators for ISAC system are described in [16], where the data rate is used for communication system and the radar estimation information rate is used for radar system. The benefits of joint sensing and communication over different approaches are illustrated in [17]. The feasibility of using 5G waveform for sensing is proved by the pioneer hardware testbed in [18] using the 5G New Radio (NR) frame structure enabled ISAC, where a novel integrated waveform enabled smart time and frequency

Manuscript received August 23, 2021; revised December 10, 2021; accepted January 14, 2022. Date of publication March 4, 2022; date of current version June 17, 2022. This work was supported in part by the National Natural Science Foundation of China (NSFC) under Grant 62022020 and Grant 61941102 and in part by the National Key Research and Development Project under Grant 2020YFB1807600. *(Corresponding author: Zhiyong Feng.)*

The authors are with the Key Laboratory of Universal Wireless Communications, Ministry of Education, Beijing University of Posts and Telecommunications, Beijing 100876, China (e-mail: zhangqixun@bupt.edu.cn; sunhz@bupt.edu.cn; xinye.gao@bupt.edu.cn; xinna_wang@bupt.edu.cn; fengzy@bupt.edu.cn).

Color versions of one or more figures in this article are available at https://doi.org/10.1109/JSAC.2022.3155506.

Digital Object Identifier 10.1109/JSAC.2022.3155506

resource filling (STFRF) algorithm and a smart weighted grid searching (SWGS) based fast beam alignment and beam tracking algorithm are designed to support flexible sensing and communication time-frequency resource configuration in [18]. And field test results verified that the ISAC system can achieve an acceptable target detection performance as well as a stable data rate for communication by using a flexible time-frequency resource allocation between sensing and communication functions in the 28 GHz mmWave frequency band for the autonomous driving vehicles (ADVs) scenario.

In terms of the signal processing of ISAC system, a multi-beam framework using steerable analog antenna arrays is designed in [19], which can achieve the seamless integration of communication and sensing. The dual-function multiple-input multiple-output (MIMO) radar and multiuser MIMO communication transmitter are proposed in [20], which can achieve a high radar performance under reasonable communication performance constraints. An adaptive joint communication and radar (JCR) virtual waveform is designed to improve the accuracy of speed estimation at the cost of a small reduce of communication data rate in [21]. From the perspective of information theory, an adaptive orthogonal frequency division multiplexing (OFDM) ISAC waveform is proposed based on the conditional mutual information (MI) and frequency selective fading channel data information rate (DIR) in [22]. Moreover, the spectrum sharing technology using ISAC design may solve the low latency raw sensing data sharing problem and improve the sensing ability of vehicles in [23]. By considering the multiuser interference (MUI) and useful MUI power tradeoff to reduce the transmit power, an efficient transmission can be achieved under the coexistence of MIMO radar and downlink multi-user multiple-input single-output (MISO) system [24]. The joint design of MIMO radar with co-located antennas and MIMO communication system is considered in [25]. To reduce the interference caused by communication systems on the accuracy of radar target localization, the co-design of radar waveform and communication transmit weights is proposed in [26] by minimizing the Cramr-Rao Bound (CRB) of direction-of-arrival (DOA) estimation In co-existence of collocated MIMO radar and downlink MISO communication systems. Furthermore, the joint transmitting design for coexistence of a MIMO communication system and sparse sensing radars in clutter is proposed in [27], where both radar and communication systems use transmit precoding to maximize the radar SINR while meeting certain communication rate and power constraints.

However, existing V2X communication technology can not support the low latency and high data rate demands for raw sensing data sharing among CAVs. And the existing research works have not considered the utilization of Sub-6GHz and mmWave spectrum bands for ISAC. The high latency and unstable V2V link become the bottlenecks for ISAC system in [28]. Therefore, the time-division enabled ISAC (TD-ISAC) system is proposed with a flexible time-frequency resource configuration ability for sensing and communication dual functions in this paper, in order to minimize the overhead of raw sensing data sharing among CAVs. To further reduce the transmission delay, the mobile edge computing (MEC) server can be deployed in vehicle and RSU equipments to process the sensing data [29]. The raw sensing data can be processed locally in vehicle or offloaded to other vehicles and road side unit (RSU), which are defined as two transmission modes, namely V2V mode and V2V/V2I collaborative mode. The response delay of sensing data transmission is analyzed theoretically under V2V mode or V2V/V2I collaborative mode among CAVs. And the closed-form solution of different communication links selection threshold is achieved with the lowest delay. And the vehicle status updating algorithm based on age of information (AoI) is also proposed to guarantee the time-sensitive service requirements in CAVs. The main contributions of this paper are summarized as follows.

- A TD-ISAC system is designed for 5G mmWave enabled CAVs in this paper. And the 5G NR based dynamic frame structure for TD-ISAC is proposed, so that each vehicle can allocate a time-frequency ratio for sensing and communication dual functions according to various demands of CAVs. Based on the proposed TD-ISAC frame structure and the interference analysis, the response time delay of a single vehicle under V2V or V2V/V2I cooperative modes is theoretically derived using First-Come-First-Served (FCFS) M/M/1 queuing theory. We analyze the response time delay of V2V and V2V/V2I modes under different maximum queue lengths.
- According to different service requirements, vehicles are defined by two types, which are the environment sensing service support (ESSS) vehicles and the cooperative vehicle infrastructure service support (CVISS) vehicles. The AoI of CVISS vehicles is proposed to guarantee the low latency raw sensing data sharing. A status update strategy to minimize AoI is designed and the closed-form solutions of AoI are achieved under different service rates.
- To verify the feasibility of TD-ISAC and the performance of V2V mode and V2V/V2I cooperative mode selection, both software simulation and hardware testbed of 5G mmWave enabled ISAC system are designed and developed in this paper. Simulation results denote that an efficient mode selection can greatly reduce the response time delay of vehicles under different queue lengths. Hardware testbed results verify effectiveness of the proposed TD-ISAC system, where the position error of target detection can be reduced by 18.5 % using the sensing data fusion from two vehicles, while a stable data rate over 2.2 Gbps can be achieved at the same time.

The rest of this paper is organized as follows. We first introduce the system model of the proposed TD-ISAC system in Section II. Then, the response delay of raw sensing data sharing among vehicles and RSU is analyzed in Section III. Section IV presents the status updating algorithm for CVISS vehicle to minimize AoI. Simulation results are shown in Section V and hardware testbed results are discussed in Section VI. Conclusions are provided in Section VII.

II. System Model

Feature sharing and result sharing are most-adopted methods for map fusion among large-scale CAVs [30]. However,

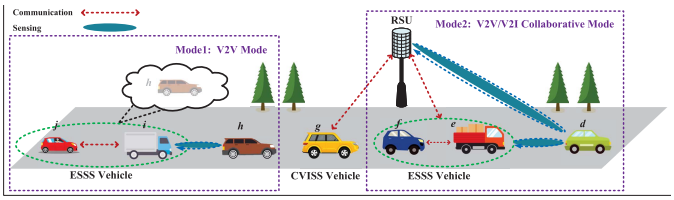

Fig. 1. Typical scenario of TD-ISAC enabled CAVs.

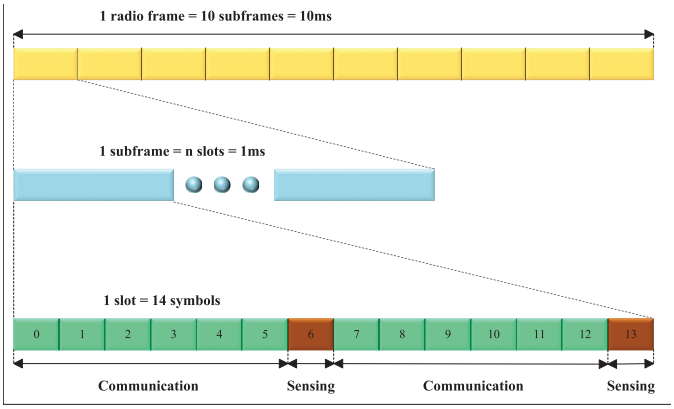

Fig. 2. The flexible sensing and communication frame structure of the proposed TD-ISAC.

in terms of the susceptible perception data from various sensors, the raw sensing data sharing among CAVs should be considered to guarantee the effective sensing data fusion and utilization for the Level 5 full automation [31]. Once a traffic accident occurs, the accident responsibility can be achieved by [32]. Because, the raw sensing data sharing can help to reduce the further spread of decision-making errors by other CAVs.

In order to improve the driving safety of ADVs, a variety of onboard sensors need be employed. However, the raw data generated by the cameras will exceed 40 Gbps [33], [34], and existing vehicle communication technologies cannot support this high data rate service demand for the time being [2]. MmWave frequency band has the characteristic of large bandwidth, and mmWave enabled V2X communications can achieve a higher data rate to support the demand of raw sensing data transmission among vehicles. Therefore, the 28 GHz mmWave frequency band is chosen to perform the sensing and communication dual functions for the ADVs scenario in ITU [49]. The typical scenario of the proposed TD-ISAC enabled CAVs in this paper is shown in Fig. 1, which consists of one RSU and multiple vehicles equipped with TD-ISAC functions. And each vehicle carries out the sensing and communication functions in a time-division manner in the proposed TD-ISAC system. Based on the flexible 5G NR frame structure defined in 3GPP [35], the sensing frames can be inserted into the communication frames to realize a flexible resource occupancy for sensing and communication in terms of different requirements on the positioning accuracy for sensing and the throughput for communication.

As shown in Fig. 2, each radio frame lasts for 10 ms, which contains 10 subframes with 1ms duration each. According to the subcarrier spacing, each subframe may contain 1, 2, 4, 8, 16 time slots, where each time slot contains 14 symbols

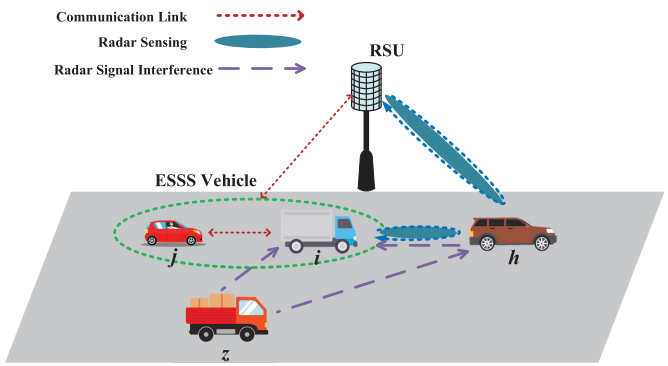

Fig. 3. Scenario of V2V/V2I collaborative mode for ESSS vehicle.

from 0 to 13. For example, symbols 0 to 2 and 7 to 9 may perform the V2V communication function. And symbols 3 to 5 and 10 to 12 may perform the V2I communication function. Specifically, symbols 6 and 13 can be allocated for the sensing function. Moreover, the ratio of time slots allocation for sensing and communication functions can also be changed dynamically according to different service requirements. In the TD-ISAC system, vehicles are divided into two types, which are ESSS vehicles and CVISS vehicles. The former ESSS vehicles are responsible for the transmission of emergency sensing data among vehicles, and the latter CVISS vehicles are responsible for the transmission of instruction information between vehicles and RSU. ESSS vehicles appear in pairs, consisting of a sending vehicle i and a receiving vehicle j, as shown in Fig. 3. Vehicle i will send and receive the sensing data in a time-division manner. Vehicle i will obtain the sensing data of vehicle h in front and share this raw sensing data with vehicle j behind in order to improve the sensing ability of vehicle j via communication links. CVISS vehicles only communicate with RSU and upload the entertainment and signaling information via V2I uplink. Then, the RSU carries out sensing function and broadcasts the sensing data to its surrounding vehicles.

As showed in Fig. 1, we proposed two communication modes, namely the mode 1 of V2V mode and the mode 2 of V2V/V2I collaborative mode, for the raw sensing data sharing among vehicles and RSU in the proposed TD-ISAC system in this paper. In mode 1, when the number of tasks arriving at vehicle i is greater than its maximum task processing capacity, vehicle i will assign part of the tasks to vehicle j for distributed processing, to alleviate the shortage of processing capability and improve the efficiency of cooperative sensing data processing. In mode 2, RSU will send the raw sensing data to vehicle i and vehicle j, which can integrate their own sensing data with the sensing data received from RSU to improve sensing range and sensing accuracy.

In this paper, we define the set of ESSS vehicles as $\mathcal{K} = \{1, 2, \ldots, K\}$, and CVISS vehicles as $\mathcal{M} = \{1, 2, \ldots M\}$, $K \gg M$. The total bandwidth resources are divided into R blocks, which are $\mathcal{R} = \{1, 2, \ldots, R\}$. The total time resources are divided into S blocks. CVISS and ESSS vehicles can share the same frequency or duration, but the resource blocks occupied by ESSS vehicles are independent. We use the indicator $a_{m,r} \in \{0, 1\}$ to denote whether the bandwidth

resource block r is allocated to CVISS vehicle m, if so, $a_{m,r} = 1$; otherwise, $a_{m,r} = 0$. Similarly, $b_{k,r} \in \{0, 1\}$ represents whether the bandwidth resource block r is allocated to the ESSS vehicle pair k, if so, $b_{k,r} = 1$; otherwise, $b_{k,r} = 0$. The $c_s \in \{0, 1\}$ $(s \in \{1, 2, \ldots, S\})$ represents whether two vehicles are in the same duration, if so, $c_s = 1$; otherwise, $c_s = 0$.

In terms of ESSS vehicle pair, vehicle i will send and receive the sensing data in a time-division manner, while vehicle j receives the sensing data from vehicle i for distributed sensing data processing cooperation. When vehicle i performs the sensing function, it will be interfered by the sensing and communication signals in the proposed ISAC system from other ESSS vehicles in the same frequency band and during the same time period. The signal to interference plus noise ratio (SINR) can be expressed by Γ_i^{rad} [36], [37]

$$\Gamma_i^{rad} = \frac{P_i h_{i,i}^t}{\Gamma_i^{r-rad} + \Gamma_i^{r-com} + N_0 W}, \tag{1}$$

$$\Gamma_i^{r-rad} = \sum_{z \in \mathcal{K}, z \neq i} \sum_{r \in \mathcal{R}} \sum_{s=1}^{S} b_{z,r} c_s P_z h_{i,z}^t, \tag{2}$$

$$\Gamma_i^{r-com} = \sum_{z \in \mathcal{K}, z \neq i} \sum_{r \in \mathcal{R}} \sum_{s=1}^{S} b_{z,r} c_s P_z G_t g_{z,i} G_r, \tag{3}$$

where Γ_i^{r-rad} represents the interference from sensing signal of other ESSS vehicles, and Γ_i^{r-com} represents the interference from communication signal of other ESSS vehicles. $b_{z,r}$ represents whether the bandwidth resource block r is allocated to the ESSS vehicle pair z, if so, $b_{z,r} = 1$; otherwise, $b_{z,r} = 0$. c_s represents whether two vehicles are in the same duration, if so, $c_s = 1$; otherwise, $c_s = 0$. P_i and P_z represent the transmit power of vehicle i and interference vehicle z, respectively. $h_{i,i}^t$ represents the channel gain of the sensing signal of vehicle i, and $h_{i,z}^t$ represents the sensing signal emitted by other vehicles which passes through the target and then refracts to the sensing signal channel gain of vehicle i [37], [38]. $g_{z,i}$ represents the communication channel gain of vehicle z in the other ESSS vehicle pair to vehicle i. N_0 is the power spectral density of thermal noise, and W is the bandwidth. Therefore, the sensing ability using ISAC can be denoted by the total radar mutual information amount of vehicle i by

$$I_i^{rad}\left(y; h_{i,i}^t\right) = a \cdot T \cdot W \log_2\left(1 + \Gamma_i^{rad}\right), \tag{4}$$

where y is the received radar signal, a is the ratio of sensing and communication time allocation, and T is the length of a frame.

When vehicle j communicates with vehicle i, it will be interfered by other vehicles. The SINR of vehicle j can be expressed as Γ_j^{com}

$$\Gamma_j^{com} = \frac{P_i G_t g_{i,j} G_r}{\Gamma_j^{c-com} + \Gamma_j^{c-rad} + N_0 W}. \tag{5}$$

where Γ_j^{c-com} represents the interference from communication signal of other ESSS vehicles, and Γ_j^{c-rad} represents the interference from radar signal of other ESSS vehicles.

$$\Gamma_j^{c-com} = \sum_{z \in \mathcal{K}, z \neq j} \sum_{r \in \mathcal{R}} \sum_{s=1}^{S} b_{z,r} c_s P_z G_t g_{z,j} G_r. \tag{6}$$

$$\Gamma_j^{c-rad} = \sum_{z \in \mathcal{K}, z \neq j} \sum_{r \in \mathcal{R}} \sum_{s=1}^{S} b_{z,r} c_s P_z \frac{G_t G_r \lambda^2}{(4\pi)^2 d_{i,z}^2}. \tag{7}$$

And, G_t and G_r represent the antenna gain at transmitter and reciever, respectively. $g_{i,j}$ is the communication channel gain between vehicle i and j, and $g_{z,j}$ is the communication channel gain between vehicle z and vehicle j. λ is the wavelength, and $d_{j,z}$ is the distance between vehicle z and vehicle j. Based on the SINR at vehicle j, the channel capacity of communication link between vehicle i and vehicle j can be defined as

$$C_{i,j} = W \cdot \log_2(1 + \Gamma_j^{com}). \tag{8}$$

When vehicle j communicates with RSU, it will be interfered by communication signals from other vehicles using the same bandwidth resource block. Thus, the SINR of vehicle j can be expressed as $\Gamma_{j,B}$

$$\Gamma_{j,B} = \frac{P_j g_{j,B}}{\sum\limits_{k \in \mathcal{K}, k \neq j} \sum\limits_{r \in \mathcal{R}} b_{k,r} P_k g_{k,B} + N_0 W}, \tag{9}$$

where P_j is the transmit power of vehicle j, and $g_{j,B}$ is the communication channel gain from vehicle j to RSU. Therefore, the channel capacity of the communication link between vehicle j and RSU can be obtained as

$$C_{j,B} = W \cdot \log_2(1 + \Gamma_{j,B}). \tag{10}$$

When the CVISS vehicle communicates with RSU through uplink, it will be interfered by the signals from other ESSS vehicles that share the same bandwidth resource block. The SINR can be expressed as Γ_m

$$\Gamma_m = \frac{P_m g_{m,B}}{\sum\limits_{k \in \mathcal{K}} \sum\limits_{r \in \mathcal{R}} a_{m,r} b_{k,r} P_k g_{k,B} + N_0 W}, \tag{11}$$

where P_m is the transmit power of CVISS vehicle, $g_{m,B}$ is the channel gain between CVISS vehicle and RSU, $g_{k,B}$ is the channel gain between the vehicle in the kth ESSS vehicle pair and RSU, and P_k is the transmit power of interference vehicle k. Therefore, the channel capacity between CVISS vehicle and RSU is denoted as

$$C_{m,B} = W \cdot \log_2(1 + \Gamma_m). \tag{12}$$

III. Response Delay Analysis

In order to analyze the response delay of the raw sensing data sharing between vehicle and RSU, we consider both V2V mode and V2V/V2I cooperative mode. Considering that the channel changes rapidly due to the fast movement of vehicles, we refer to the existing research works on the fast time-varying channel estimation [39], [40]. In this paper, based on the accurate fast time-varying channel estimation, the response delay analysis of V2V and V2V/V2I modes is proposed in two subsections in detail. And the theoretical solutions of threshold for V2V mode and V2V/V2I collaborative mode selection are achieved in this section.

A. Response Delay Analysis for Mode 1: V2V Mode

In order to analyze the response time delay of distributed vehicle cooperation, the $M/M/1/N$ queuing theory model is used in this paper [41], [42]. The packet received at vehicle i is approximately regarded as a Poisson process with an arrival rate of Λ_i, and the processing rate is μ. Therefore, the calculation load rate of vehicle i is defined by $\rho_i = \Lambda_i/\mu$, and the maximum task capacity of vehicle i is defined as N_i.

Thus, the average number of tasks L_i in the computation system of vehicle i can be obtained by

$$L_i = \sum_{n=0}^{N_i} np_n = \frac{\rho_i}{1-\rho_i} - \frac{(N_i+1)(\rho_i)^{N_i+1}}{1-(\rho_i)^{N_i+1}}, \quad (13)$$

where p_n represents the probability that there are n tasks and p_n is denoted by

$$p_n = \begin{cases} \dfrac{(1-\rho)\rho^n}{1-\rho^{N+1}}, & \rho \neq 1,\ 1 \leq n \leq N \\ \dfrac{1}{N+1}, & \rho = 1. \end{cases} \quad (14)$$

As shown in Fig. 3, when the sensing data detected by vehicle i is relatively small, vehicle i will process the sensing data and transmit the processed information to vehicle j. For vehicle i, there is only the computation delay as denoted by T_i^{comp1}. For vehicle j, there are two kinds of delay, which are the calculation delay generated by vehicle i denoted by T_i^{comp1}, and the transmission delay from vehicle i to vehicle j denoted by $T_{i,j}$. At this point, the calculation delays of vehicle i and vehicle j are defined by T_i, T_j, respectively.

$$T_i = T_i^{comp1}, \quad (15)$$

$$T_j = T_i^{comp1} + T_{i,j}, \quad (16)$$

where T_i^{comp1} represents the calculation delay of vehicle i, $T_{i,j}$ represents the transmission delay from vehicle i to vehicle j. According to the Littles law of queuing theory, when the number of tasks is less than the maximum task capacity, the computing delay of the system can be denoted by

$$T_i^{comp1} = \frac{L_i}{\Lambda_i}. \quad (17)$$

The total amount of sensing data detected by radar is defined as l. Combined with the analysis of the channel capacity $C_{i,j}$ of the communication link between vehicle i and vehicle j, the transmission delay is obtained as

$$T_{i,j} = \frac{l}{C_{i,j}}. \quad (18)$$

When the sensing data detected by vehicle i is relatively large, the number of tasks is more than the maximum task capacity, where the system cannot process all the arriving tasks. At this point, the number of tasks in the computing server of vehicle i is equal to the maximum task capacity of the computing server N, and p_n is recorded as P_{N_i} which represents the rejection probability of the arriving tasks by the computing server. Therefore, the tasks that can not be processed by vehicle i will be cooperatively processed by vehicle j with the task arrival rate of Λ_j

$$\Lambda_j = \Lambda_i P_{N_i}, \quad (19)$$

where ρ_j represents the calculation load rate of vehicle i, L_j represents the average number of tasks existing in the calculation system of vehicle j, and N_j represents the maximum task capacity of vehicle j.

$$\rho_j = \frac{\Lambda_j}{\mu}, \quad (20)$$

$$L_j = \sum_{n=0}^{N_j} np_n = \frac{\rho_j}{1-\rho_j} - \frac{(N_j+1)(\rho_j)^{N_j+1}}{1-(\rho_j)^{N_j+1}}. \quad (21)$$

According to Little Theorem of queuing theory, when the number of tasks in the system is bigger than the maximum task capacity, the computing delay of the vehicle i and vehicle j can be denoted by T_i^{comp2} and T_j^{comp}, respectively.

$$T_i^{comp2} = \frac{L_i}{\Lambda_i(1-P_{N_i})} = \frac{L_i(1-(\rho_i)^{N_i+1})}{\Lambda_i(1-(\rho_i)^{N_i})}, \quad (22)$$

$$T_j^{comp} = \frac{L_j}{\Lambda_j} = \frac{L_j}{\Lambda_i P_{N_i}} = \frac{L_i\left(1-\rho_j^{N_j+1}\right)}{\Lambda_i(1-\rho_j)\rho_j^{N_j}}. \quad (23)$$

Therefore, the sensing data detected by radar that vehicle i and vehicle j need to process are l_i and l_j, respectively.

$$l_i = \frac{lL_i}{L_i+L_j}, \quad (24)$$

$$l_j = \frac{lL_j}{L_i+L_j}. \quad (25)$$

In this case, when vehicle i generates a large amount of sensing data from high definition cameras or other sensors, it will transmit part of the sensing information to vehicle j for distributed sensing data processing cooperation. There are four kinds of delay for vehicle i, which are the calculation delay of vehicle i by T_i^{comp2}, the transmission delay of vehicle i to vehicle j by $T_{i,j}$, the calculation delay of vehicle j by T_j^{comp}, and the transmission delay of vehicle j to vehicle i by $T_{j,i}$. Similarly, for vehicle j, there are three kinds of delay, which are the calculation delay of vehicle i by T_i^{comp2}, the transmission delay of vehicle i to vehicle j by $T_{i,j}$, and the calculation delay of vehicle j by T_j^{comp}. Thus, the calculation delays of vehicle i and vehicle j are denoted by T_i and T_j, respectively.

$$T_i = T_i^{comp2} + T_{i,j} + T_j^{comp} + T_{j,i}, \quad (26)$$

$$T_j = T_i^{comp2} + T_{i,j} + T_j^{comp}, \quad (27)$$

where $T_{i,j} = \frac{l_i}{C_{i,j}}$, and $T_{j,i} = \frac{l_j}{C_{j,i}}$.

In this paper, the response delay denoted by (15) and (16) is called the full response delay (FRD) for vehicle i and vehicle j. And, the response delay in (26) and (27) is called the overload response delay (ORD) for vehicle i and vehicle j.

B. Response Delay Analysis in Mode 2: V2V/V2I Collaborative Mode

In Fig. 3, ESSS vehicles will receive the sensing data from RSU via the V2V/V2I collaborative mode. When the sensing data detected by vehicle i is large, vehicle i will transmit part of the sensing data to RSU for cooperation.

Therefore, we first analyze the delay when vehicle i transmits the sensing data to RSU. Since the calculation capability of RSU is not a problem for most of the cases, we assume that the calculation delay of RSU is ignored for simplicity in this paper. For vehicle i, there are three types of time delay, which are the computation delay in vehicle i, the transmission delay from vehicle i to RSU, and the transmission delay from RSU to vehicle i. For vehicle j, there are four types of time delay, which are the computation delay in vehicle i, the transmission delay from vehicle i to vehicle j, the transmission delay from vehicle i to RSU, and the transmission delay from RSU to vehicle j.

Based on the analysis and results in Section III. A, the radar mutual information remains unchanged. When the sensing data detected by vehicle i is large, the calculation delay of vehicle i is defined by T_i^{comp2}. And the transmission delay of $T^{i,B}$, $T_{B,i}$, $T^{j,B}$, $T^{i,j}$ are denoted as

$$T_{i,B} = \frac{l_j}{C_{i,B}}, \tag{28}$$

$$T_{B,i} = \frac{l_j}{C_{B,i}}, \tag{29}$$

$$T_{B,j} = \frac{l_j}{C_{B,j}}, \tag{30}$$

$$T_{i,j} = \frac{l_i}{C_{i,j}}. \tag{31}$$

Therefore, the total response delay of sensing data sharing using the V2V/V2I collaborative mode can be written as

$$\begin{aligned} T_i &= T_i^{comp2} + T_{i,B} + T_{B,i} \\ &= \frac{L_i(1-(\rho_i)^{N_i+1})}{\Lambda_i(1-(\rho_i)^{N_i})} + \frac{2l_j}{C_{i,B}}, \end{aligned} \tag{32}$$

$$\begin{aligned} T_j &= T_i^{comp2} + T_{i,j} + T_{i,B} + T_{B,j} \\ &= \frac{L_i(1-(\rho_i)^{N_i+1})}{\Lambda_i(1-(\rho_i)^{N_i})} + \frac{l_i}{C_{i,j}} + \frac{l_j}{C_{i,B}} + \frac{l_j}{C_{B,j}}. \end{aligned} \tag{33}$$

In V2V mode, we can calculate the FRD of a pair of ESSS vehicles using (15) and (16) and the ORD of a pair of ESSS vehicles using (26) and (27). In V2V/V2I mode, we can calculate the response delay of a pair of ESSS vehicles using (32) and (33) as follows

$$T_{V2V-FRD} = 2T_i^{comp1} + T_{i,j}, \tag{34}$$

$$T_{V2V-ORD} = 2T_i^{comp2} + 2T_{i,j} + 2T_j^{comp} + T_{j,i}, \tag{35}$$

$$T_{V2V-V2I} = 2T_i^{comp2} + T_{i,j} + 2T_{i,B} + T_{B,i} + T_{B,j}. \tag{36}$$

When the system is overload, the optimal communication mode selection between mode 1 and mode 2 is crucial to guarantee the low latency of sensing data sharing among vehicles and RSU. Therefore, we can obtain the threshold of communication mode selection by subtracting (36) from (35) as

$$\begin{aligned} f(N_i, N_j, \Lambda_i) &= T_{V2V-ORD} - T_{V2V-V2I} \\ &= T_{i,j} + 2T_j^{comp} + T_{j,i} - 2T_{i,B} - T_{B,i} - T_{j,B} \end{aligned} \tag{37}$$

Furthermore, RSU can be utilized not only as processing unit but also to assist the raw sensing data sharing among vehicles in the proposed TD-ISAC system. By equipped with different types sensors such as the camera in RSU, it can establish and maintain the mmWave communication links for vehicles in [43]. Besides, due to the sensing ability limitation of one vehicle, RSU can act as a fixed node to detect the surrounding vehicles and increase the detection accuracy. As shown in Fig. 1, RSU can deliver the sensing data about vehicle d to vehicle e. Then, vehicle e integrates the sensing information of vehicle d detected by itself and received from RSU to improve the detection accuracy via sensing data fusion. To verify the effectiveness of sensing data fusion, the hardware testbed of TD-ISAC system is designed and the improvement of detection accuracy is discussed in Section VI.

IV. CVISS Vehicle Status Update Algorithm

Because CVISS vehicles do not exchange information directly with other ESSS vehicles, they will not be able to flexibly adapt to the time sensitive service due to the lack of sufficient sensing information. To solve this problem, a status update algorithm based on AoI is proposed for CVISS vehicles in this section to guarantee the low latency raw sensing data sharing. The closed-form solutions of AoI are also achieved under different service rates.

A. AoI Analysis of CVISS Vehicles

AoI is an indicator to denote the freshness of information, which is very important for the low latency raw sensing data sharing between CVISS vehicles and RSU in this paper. The smaller the value of AoI, the better the performance of corresponding vehicles for the timeliness of sensing data transmission.

The system of the CVISS vehicles is modeled as the first-come-first-service model $M/M/1/N$. When the capacity of the vehicle MEC server is N, AoI can be expressed as a function of μ and ρ [44], [45],

$$\Delta_{M/M/1/N} = f_2(\mu, \rho). \tag{38}$$

For example, when the capacity of vehicle's MEC server N equals to 1 and 2, $\Delta_{M/M/1/1}$ and $\Delta_{M/M/1/2}$ can be expressed as

$$\Delta_{M/M/1/1} = \frac{1}{\Lambda} + \frac{2}{\mu} - \frac{1}{\Lambda+\mu}, \tag{39}$$

$$\Delta_{M/M/1/2} = \frac{1}{\Lambda} + \frac{3}{\mu} - \frac{2(\Lambda+\mu)}{\Lambda^2+\Lambda\mu+\mu^2}. \tag{40}$$

Since $\rho = \frac{\lambda}{\mu}$, (39) and (40) can be written as

$$\Delta_{M/M/1/1} = \frac{1}{\mu}(\frac{1}{\rho} + 2 - \frac{1}{1+\rho}), \tag{41}$$

$$\Delta_{M/M/1/2} = \frac{1}{\mu}[\frac{1}{\rho} + 3 - \frac{2(1+\rho)}{\rho^2+\rho+1}]. \tag{42}$$

According to (41) and (42), it can be inferred that the relative size of AoI under different capacities is only affected by ρ. And, the capacity of vehicle's MEC server can be adjusted according to the calculation load rate of vehicle to

minimize the AoI. The capacity of vehicle's MEC server can be adjusted from 1 to N_c, where N_c is the maximum capacity of vehicle's MEC server. The vehicle can calculate the current average load rate at intervals t and adjust the capacity of vehicle's MEC server based on the calculation load rate to minimize AoI,

$$\bar{\rho} = \frac{U}{\mu t}, \tag{43}$$

$$N = \underset{n \in Z, n \in [1, N_c]}{arg\min} \Delta_{M/M/1/n}, \tag{44}$$

where $\bar{\rho}$ is the average calculation load rate within time t, and U represents the number of tasks received within time t.

When the capacity of vehicle's MEC server is n, the state is denoted as

$$R_n = f_3\left(\Lambda, \mu, N = n\right). \tag{45}$$

B. Status Update Algorithm Based on AoI

CVISS vehicles have relatively independent functions, with V2I communication function, but not with sensing function and V2V function. They cant exchange information directly with other ESSS vehicles. As a result, CVISS vehicles lack sufficient environmental sensing information to update their computational models and are unable to adapt flexibly to time-sensitive services. Therefore, a status update algorithm based on AoI is proposed for CVISS vehicles in this subsection. Federated learning algorithm is used to collect sensor data from distributed ESSS vehicles to ensure the protection of privacy information. Each ESSS vehicle will send the information it perceives to RSU. RSU will summarize the environmental sensing information and send it to CVISS vehicles to solve the environmental sensing problem of CVISS vehicles. In (43), CVISS vehicles estimate their own task arrival rate by calculating the average task arrival rate within this period of time at intervals, so that the arrival rate obtained is obviously lagging in time. Therefore, we consider a method to estimate the task arrival rate of CVISS vehicles by RSU. Considering that the closer an ESSS vehicle is to the CVISS vehicle, the more useful its environmental sensing information is to the CVISS vehicle. Therefore, we consider the CVISS vehicle calculation load rate estimation based on inverse distance weighting based k-nearest neighbor classification algorithm, which is convenient for CVISS vehicles to make decisions to minimize AoI.

First, ESSS vehicles upload environmental sensing information to RSU via V2I link. Then, RSU processes the information and weighted average the key parameters of ESSS vehicles to calculate the calculation load rate of CVISS vehicles. The key parameters include ESSS vehicle number, distance between ESSS vehicle and CVISS vehicle, ESSS vehicle task arrival rate. Finally, RSU sends the processed environmental sensing information to CVISS vehicles and weights the parameters to facilitate CVISS vehicles to estimate their own calculation load rate. The weights are determined by the distance between ESSS vehicles and CVISS vehicles through inverse distance weighting based k-nearest neighbor classification algorithm.

The CVISS vehicle status update algorithm is described in **Algorithm 1**. RSU first carries out the weighted average process on the collected model parameters, and then takes the calculation load rate result as current state of the CVISS vehicle. Next, the AoI is calculated as the vehicle capacity is selected from 1 to N_c, which is used to determine whether the status of CVISS needs to update or not. It is also assumed that there are k ESSS vehicles participating in the parameter uploading, and the distance between each ESSS vehicle and CVISS vehicle is defined by d. Therefore, the result of the status update can be expressed as

$$R \leftarrow \frac{\sum_{i=1}^{k} \Lambda_i \frac{1}{d}}{\mu \sum_{i=1}^{k} \frac{1}{d}} \leftarrow \frac{\sum_{i=1}^{k} f_i(\Lambda_i, \mu, N) \frac{1}{d}}{\sum_{i=1}^{k} \frac{1}{d}}. \tag{46}$$

Algorithm 1 CVISS Vehicle Status Update Algorithm

Input: System status parameter information for each ESSS vehicle pair.
Output: Update model of CVISS vehicle.
Step 1: Calculate the system update parameter ρ^*.
Randomly obtain the distance information d of k vehicles to form set K.
for each $i \in K$ **do**
The computing system of RSU calculates $\rho^* = \frac{\sum_{i=1}^{k} \Lambda_i \frac{1}{d}}{\mu \sum_{i=1}^{k} \frac{1}{d}}$.
end for
Step 2: Status update of CVISS vehicle.
Calculate $\Delta_{M/M/1/1}$, $\Delta_{M/M/1/2} \ldots \Delta_{M/M/1/N_c}$ according to ρ^*.
for each round t=0,1,2,..., **do**
  if $\Delta_{M/M/1/n} = \min\left\{\Delta_{M/M/1/1}, \ldots, \Delta_{M/M/1/N_c}\right\}$ **then**
    $R_n \leftarrow \frac{\sum_{i=1}^{k} \Lambda_i \frac{1}{d}}{\mu \sum_{i=1}^{k} \frac{1}{d}} \leftarrow \frac{\sum_{i=1}^{k} f_i(\Lambda_i, \mu, N) \frac{1}{d}}{\sum_{i=1}^{k} \frac{1}{d}}$.
  end if
end for
Save R.

V. Simulation Results and Analysis

In this section, the performance of the proposed TD-ISAC system in terms of the response time delay is evaluated by simulation results by considering both V2V mode and V2V/V2I collaboration mode. We also assume that the proposed TD-ISAC system can share the hardware equipment and signal processing resources for sensing and communication. Therefore, in the simulation, we evaluate the feasibility of the proposed TD-ISAC functions based on the 5G NR frame structure. Specifically, the antenna gains of transmitter and receiver are set by G_t and G_r with the same value of 18 dB. The carrier frequency at 28 GHz is considered in the simulation with a bandwidth of 800 MHz [17]. The transmit power of each vehicle in the simulation is set to 40 dBm (10 W) [47], [48]. In the simulation, 10 ESSS vehicles and 2 CVISS vehicles are considered. The path loss is $PL\,(\text{dB}) = 20\log_{10}\left(\frac{4\pi f}{c}\right) + 10n\log_{10}(d) + \chi_\sigma^{CI}$ [46], where

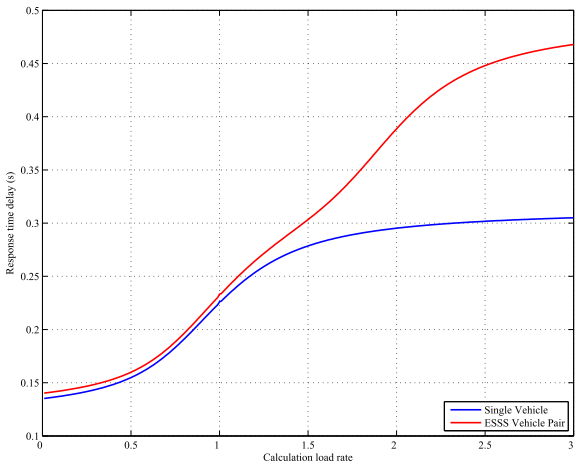

(a)

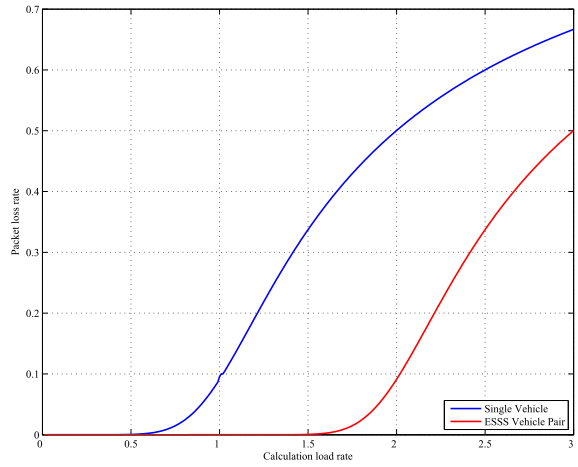

(b)

Fig. 4. Performance comparison between single vehicle and ESSS vehicle pair. (a) Response time delay, (b) Packet loss rate.

n is 2, and χ_{σ}^{CI} is the standard deviation of shadow fading and set to 5. The detailed parameters and settings of the proposed simulation system are shown in TABLE I.

Fig. 4 shows both the response time delay and the packet loss rate of single vehicle and ESSS vehicle pair under different calculation load rate conditions. In Fig. 4(a), results depict that when the calculation load rate is less than 1.5, the response delay of single vehicle and ESSS vehicle pair is similar. But, when the calculation load rate is greater than 1.5, the response delay of ESSS vehicle pair is significantly higher than that of single vehicle. In Fig. 4(b), when the calculation load rate is higher than 1, the packet loss rate is much higher for single vehicle than ESSS vehicle pair. For ESSS vehicle pair, the packet loss rate increases significantly when the calculation load rate is higher than 1.5. Therefore, V2V mode can greatly reduce the packet loss rate at the expense of a small delay when the calculation load rate is greater than 0.5. Therefore, when the current vehicle receives a large number of tasks, the proposed V2V and V2V/V2I communication modes can be selected to reduce the packet loss rate efficiently.

Assuming that the time slot occupancy of sensing function in ESSS vehicle frame structure is 1/14, 2/14, and 3/14 randomly, the simulation results of V2V-ORD and V2V-V2I delay

TABLE I

KEY SIMULATION PARAMETERS OF TD-ISAC SYSTEM

Parameter	Value
f	28 GHz
W	800 MHz
M	10
K	2
T	10 ms
P	10 W
G_t/G_r	18 dB
Path loss	$20\log_{10}\left(\frac{4\pi f}{c}\right)+20\log_{10}(d)+5$

are shown in Fig. 5. The response delay of these two modes increases monotonically with the increase of calculation load rate. The red line and blue line represent the response delay of V2V-V2I and V2V-ORD when the MEC server queue capacity N is 5, 10, 15, and 20, respectively. The intersection points of red and blue lines in these four subfigures Fig. 5(a)-(d) are important for the mode selection when N is 5, 10, 15, and 20. In Fig. 5(a), when $N = 5$, it can be seen that the response delay of V2V-V2I is smaller than that of V2V-ORD when the calculation load rate is less than 1.2. In ESSS vehicle pair, the lead vehicle assigns the task to RSU. When the calculation load rate is greater than 1.2, in ESSS vehicle pair, the front vehicle will preferentially assign tasks to the back vehicle. When the calculation load rate is greater than 1.2, the leading vehicle in ESSS vehicle pair switches the communication mode from V2V-V2I to V2V to reduce the response time delay. Similarly, in Fig. 5(b), when $N = 10$, the communication mode will be switched as the calculation load rate reaches 1.31. When the calculation load rate is less than 1.31, ESSS vehicle pair will select V2V-V2I communication mode. When the calculation load rate is greater than 1.31, ESSS vehicle pair selects V2V-ORD communication mode. In Fig. 5(c), when $N = 15$ and the calculation load rate reaches 1.21, the communication mode is switched. When the calculation load rate is less than 1.21, ESSS vehicle pair will select V2V-V2I communication mode. When the calculation load rate is greater than 1.21, ESSS vehicle pair selects V2V-ORD communication mode. In Fig. 5(d), when $N = 20$ and the calculation load rate reaches 1.6, the communication mode is switched. When the calculation load rate is less than 1.6, ESSS vehicle pair will select V2V-V2I communication mode. When the calculation load rate is greater than 1.6, ESSS vehicle pair selects V2V-ORD communication mode.

Fig. 6 shows the changes of AoI of CVISS vehicles before and after using the proposed status updating algorithm based on AoI in Section IV.B. For vehicles with capacity 1 and 2, by subtracting (39) and (40), the conclusion is that when $\rho < 0.618$, $\Delta_{M/M/1/2} < \Delta_{M/M/1/1}$. When the system capacity of vehicle is 2, the server calculation load rate will increase with the increase of task arrival rate. We assume that $\rho > 0.618$ is obtained after RSU performs the proposed status updating algorithm. Thus, RSU will decide the CVISS vehicles to update system capacity and reduce AoI, which are denoted by the intersection points of solid and dotted lines in Fig. 6. Results also show that AoI becomes smaller after using the proposed status updating algorithm than that of the original status. With the change of task arrival rate, RSU will decide

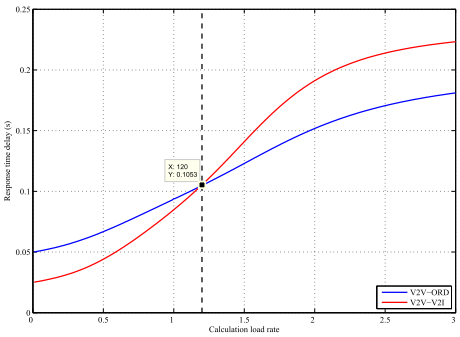

(a)

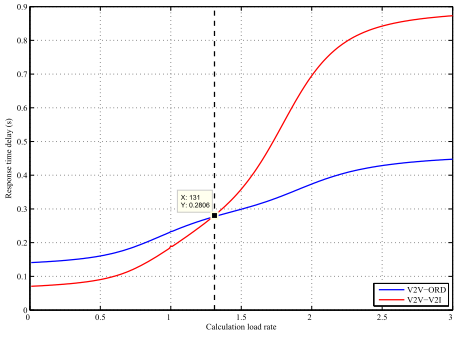

(b)

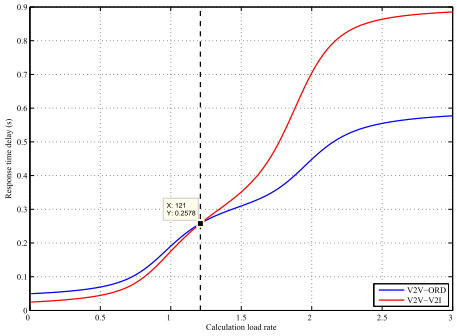

(c)

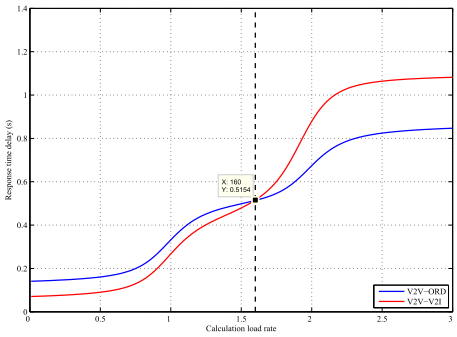

(d)

Fig. 5. Response time delay of V2V-ORD and V2V-V2I when the MEC server queue capacity N is 5, 10, 15 and 20. (a) $N = 5$, (b) $N = 10$, (c) $N = 15$, (d) $N = 20$.

whether CVISS vehicle to proceed system status updating or not, and then give new system model parameters to CVISS vehicle to achieve a new task arrival rate. In addition, it can

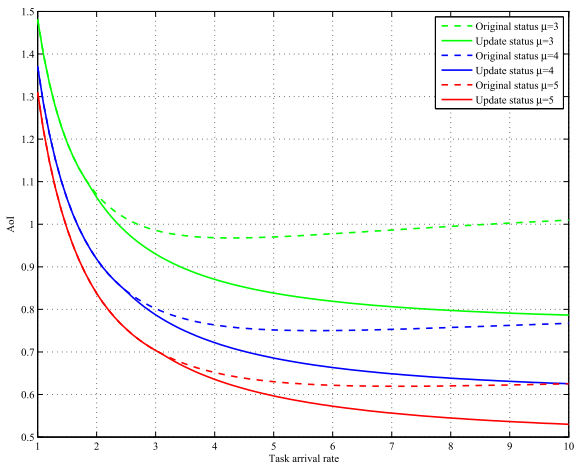

Fig. 6. Comparison of AoI before and after system status updating.

be seen from Fig. 6 that as λ increases, the solid line decreases all the time, and the dashed line decreases first and then rises. Because if we take the derivative of $\Delta_{M/M/1/1}$ and $\Delta_{M/M/1/2}$, respectively, namely the derivative of (39) and (40), we have $\frac{d\Delta_{M/M/1/1}}{d\lambda} = \frac{-\mu(2\lambda+\mu)}{\lambda^2(\lambda+\mu)^2} < 0$ and $\frac{d\Delta_{M/M/1/2}}{d\lambda} = \frac{\lambda^4+2\mu\lambda^3-3\mu^2\lambda^2-2\mu^3\lambda-\mu^4}{\lambda^2(\lambda^2+\lambda\mu+\mu^2)^2}$, when $\lambda > 0$ and $\mu > 0$. Therefore, $\Delta_{M/M/1/1}$ is monotonically decreasing and $\Delta_{M/M/1/2}$ is not monotonically decreasing.

VI. Hardware Testbed and Results of TD-ISAC System

The performance of the proposed algorithms for cooperative raw sensing data sharing among CAVs is evaluated by the mmWave enabled TD-ISAC hardware testbed as shown in Fig. 7.

The integrated baseband signal is sent from DAC module and IF module of the mmWave enabled TD-ISAC testbed, and then it is up converted by 28 GHz radio frequency (RF) head to the phased array antenna. The integrated waveform is sent out by the antenna to realize the positioning of target and the transmission of communication data simultaneously. In this testbed, two ISAC systems are set to the transceiver mode. First, ISAC system 1 and 2 send the integrated waveform of sensing and communication (IWSC) to detect the target's position. In terms of a general scenario where two ISAC systems are placed in different locations, two sets of target detection data can be obtained individually, which include target's angle and distance. Then, two ISAC systems keep the IWSC unchanged and adjust the beam angle to establish the mmWave communication link between these two ISAC systems. Specifically, ISAC system 1 can transmit its raw detection data to ISAC system 2 to realize raw sensing data fusion at ISAC system 2. Considering the limits of accuracy and resolution of target's detection for single ISAC system, the positioning results from ISAC system varies in a certain area around the real position, which can be defined as a confidence region (CR) of single ISAC system. During the sensing data fusion from two separated ISAC systems, only the positioning results within the overlapped area of two systems' CR is considered valid for further processing. As a result, compared

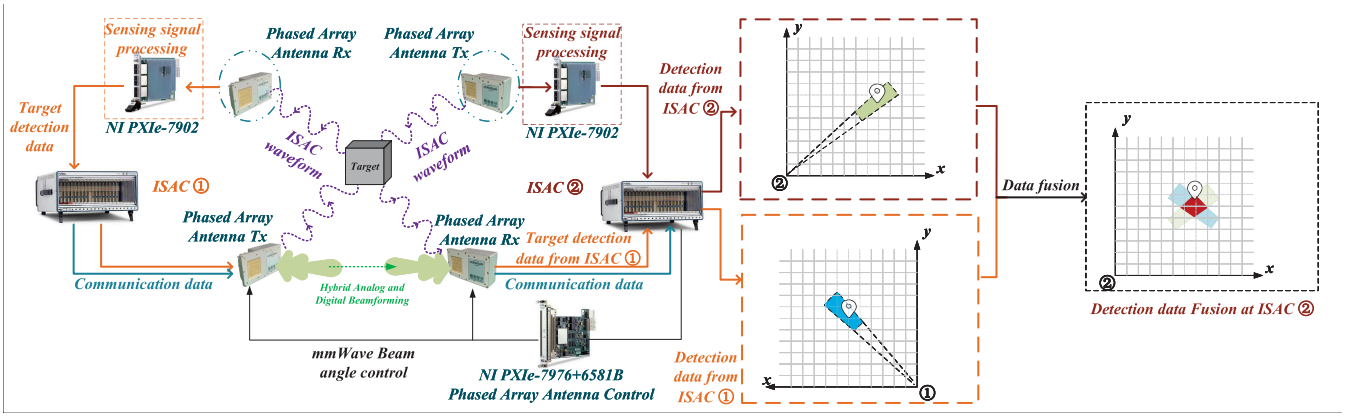

Fig. 7. Hardware testbed architecture of raw sensing data fusion for the proposed TD-ISAC system.

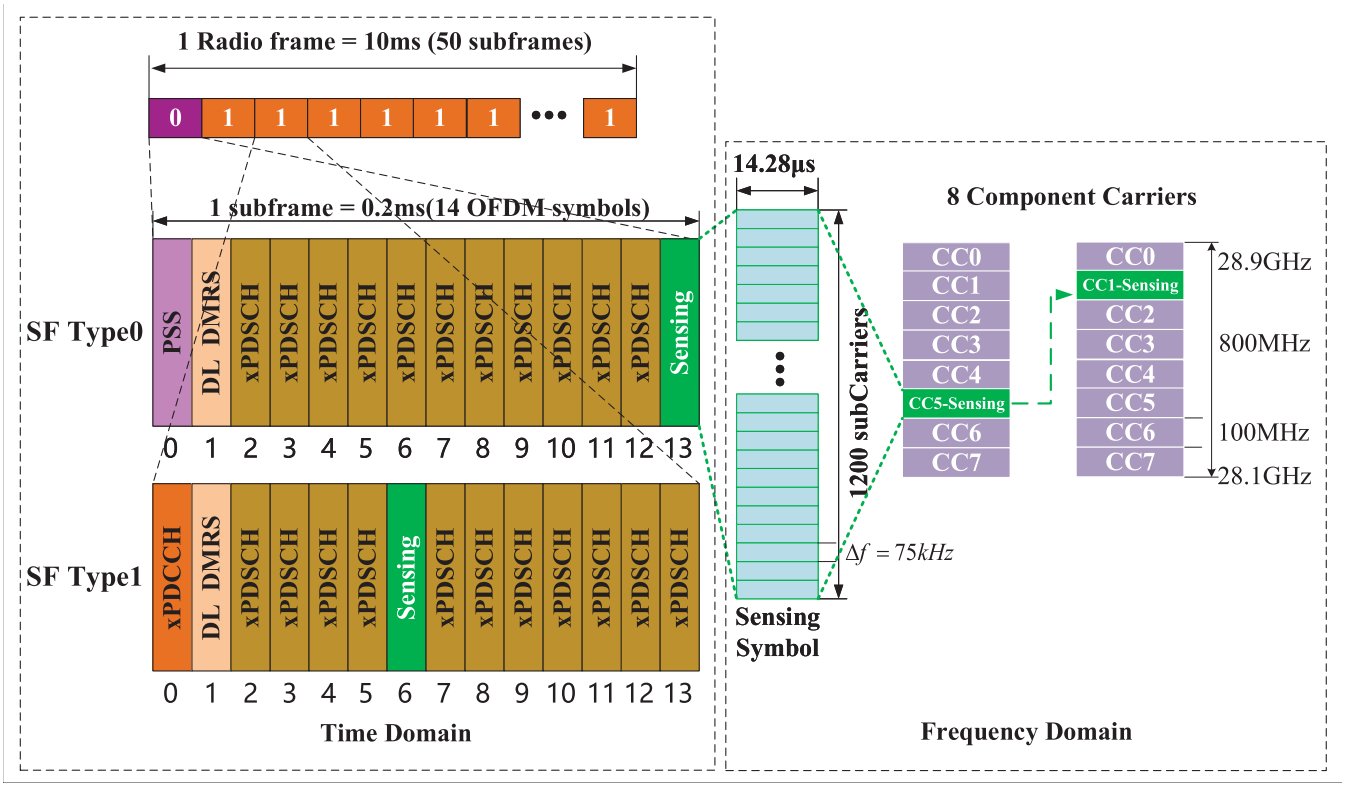

Fig. 8. Frame structure of the proposed TD-ISAC system.

with single system detection, a smaller CR and a more accurate positioning performance can be achieved.

The TD-ISAC system can flexibly adjust the ratio between sensing and communication resources in terms of different service demands. Thus, the bandwidth resources can be utilized efficiently and the channel load can be reduced. The frame structure of the proposed TD-ISAC system is presented in Fig. 8. One frame contains 50 subframes, and each subframe has a 10 ms duration. Each subframe contains 14 OFDM symbols, and each symbol carries 1200 subcarriers in the frequency domain. The carrier interval is 75 kHz. The carrier frequency of TD-ISAC hardware tested is 28.5 GHz, and the total bandwidth is 800 MHz which contains 8 component carriers. The frequency band of TD-ISAC enabled radar currently only occupies 100 MHz bandwidth, which can be enlarged to occupy 800 MHz. The frequency hopping change of radar band in 8 component carriers can be realized through parallel radar data filling, and the bandwidth occupied by the sensing function on can be flexibly adjusted. In the testbed, different configuration ratios of PDSCH for sensing and communication have been designed and realized with the performance results as follows.

The proposed TD-ISAC hardware testbed consists of two TD-ISAC system and one target in Fig. 9. Two TD-ISAC systems are placed with a distance of 5 m from each other, and constantly detect the target which is moving from left to right. TD-ISAC system 1 transmits its sensing data to TD-ISAC system 2 by using a time-division based on beam angle adjustment scheme. The receiver mounted on the target can receive the integrated waveform from TD-ISAC system 2 and demodulates the data.

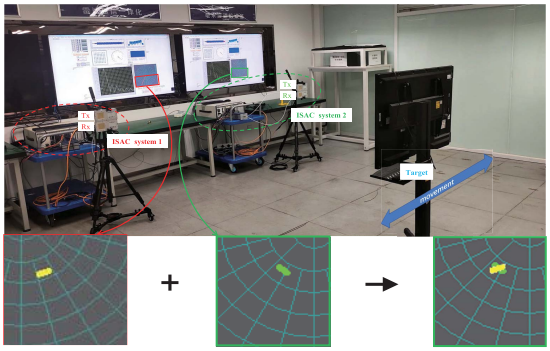

Fig. 9. Hardware testbed of the proposed TD-ISAC system.

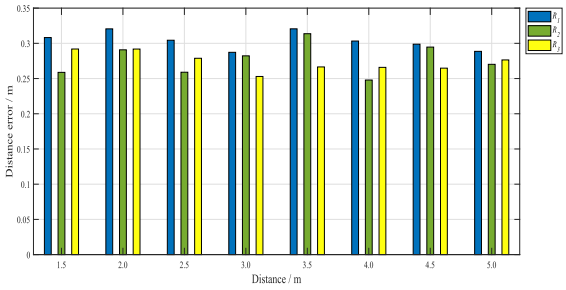

Fig. 10. Distance error of the proposed TD-ISAC system.

Both the sensing and communication performances can be obtained by changing the sensing and communication ratio in the proposed frame structure as shown in Fig. 8. Three types of sensing and communication ratio are considered and implemented in the TD-ISAC hardware testbed, which are R_1 = 1/699, R_2 = 1/13, and R_3 = 1/6. To evaluate the performance of target detection, the proposed TD-ISAC system was used for the distance and angle measurements, respectively. Figs. 10 and 11 describe the sensing performances of one TD-ISAC system without the sensing information fusion. Fig. 10 shows the distance error for 8 positions on the target trajectory under three sensing and communication ratios. The average distance error of R_1, R_2, R_3 is 0.304 m, 0.2771 m and 0.2736 m, respectively. Results indicate that a lower distance error can be achieved with a higher proportion of sensing time slot occupancy in the proposed frame structure in Fig. 8. Similarly, Fig. 11 shows the angle error for 8 positions on the target trajectory under three sensing and communication ratios. The average angle error of R_1, R_2, R_3 is 5 °, 4.37 °, and 4.25 °, respectively. Results indicate that a lower angle error can be achieved with a higher proportion of sensing time slot occupancy.

Furthermore, the sensing performance of the proposed TD-ISAC system can be improved by the sensing data fusion using two TD-ISAC systems in Fig. 9. Fig. 12 shows the positioning error for 8 positions on the target trajectory under three sensing and communication ratios. Results indicate that a higher positioning accuracy depicted by the confidence region of positioning can be achieved with a higher proportion of sensing time slot occupancy in proposed frame structure in Fig. 8. The proposed cooperative sensing ability can be improved based on the sensing data fusion, which is proved to be effective by the decrease of positioning error. Results show that the positioning error can be reduced by 18.5% on

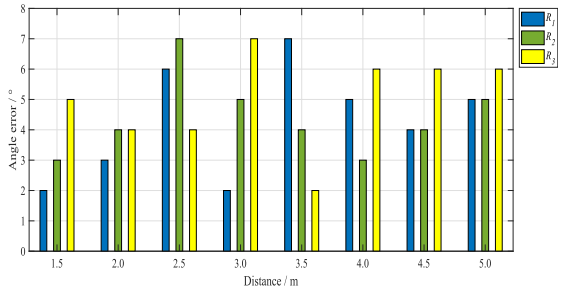

Fig. 11. Angle error of the proposed TD-ISAC system.

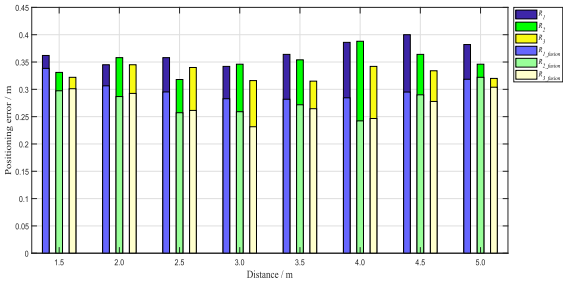

Fig. 12. Positioning error of the proposed TD-ISAC system.

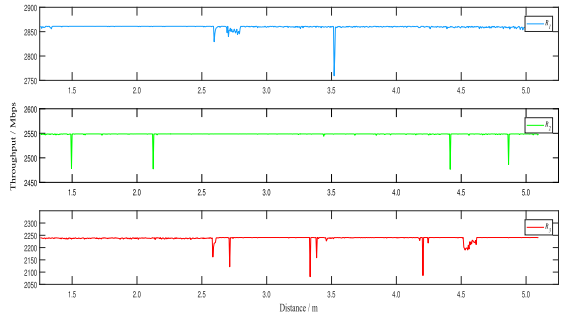

Fig. 13. Throughput of the proposed TD-ISAC system.

average for these three ratios. Moreover, we believe that the speed measurement, tracking and motion detection are very important for the proposed TD-ISAC system, which will be considered in our future work.

In terms of the communication performance of the proposed TD-ISAC system, the throughput is evaluated using the hardware testbed. The communication throughput can be remained over 2.2 Gbps as shown in Fig. 13. For three sensing and communication ratios of R_1, R_2, and R_3, the throughput remains stable at 2.86 Gbps, 2.55 Gbps, and 2.25 Gbps, respectively. Results indicate that with the increase of sensing time slot occupancy, the throughput will be reduced.

VII. Conclusion

In this paper, we have proposed the mmWave enabled CAVs cooperation algorithm for TD-ISAC system, which can minimize the response time delay of raw sensing data sharing among CAVs. The closed-form solution for V2V mode and V2V/V2I collaborative communication mode selection is theoretically achieved based on response time delay analysis, which can guarantee the timeliness of raw sensing data sharing. A novel system status update algorithm based on AoI is also proposed for CVISS vehicle under the V2V/V2I collaborative mode. The performances of the proposed

algorithms for TD-ISAC system are evaluated by simulation and hardware testbed. The proposed communication mode selection algorithm can effectively minimize the response time delay in different conditions based on simulation results. And the mmWave enabled TD-ISAC hardware testbed results show that the position error of target detection can be reduced by 18.5 % using the sensing data fusion, while the communication throughput can be remained over 2.2 Gbps. Therefore, the feasibility of the proposed algorithms for TD-ISAC system is proved by theoretical analysis and hardware testbed results in this paper.

REFERENCES

[1] W. Zong, C. Zhang, Z. Wang, J. Zhu, and Q. Chen, "Architecture design and implementation of an autonomous vehicle," *IEEE Access*, vol. 6, pp. 21956–21970, 2018.

[2] S. Liu, L. Liu, J. Tang, B. Yu, and W. Shi, "Edge computing for autonomous driving: Opportunities and challenges," *Proc. IEEE*, vol. 107, no. 8, pp. 1697–1716, Jun. 2019.

[3] L. Kong, M. K. Khan, F. Wu, G. Chen, and P. Zeng, "Millimeter-wave wireless communications for IoT-cloud supported autonomous vehicles: Overview, design, and challenges," *IEEE Commun. Mag.*, vol. 55, no. 1, pp. 62–68, Jan. 2017.

[4] *Annex 16 to Working Party 5A Chairmans Report on Working Document Towards a Preliminary Draft New Report ITU-R M.[CAV] Connected Automated Vehicles (CAV)*, International Telecommunication Union, Geneva, Switzerland, Nov. 2020.

[5] S. Chen *et al.*, "Vehicle-to-everything (v2x) services supported by LTE-based systems and 5G," *IEEE Commun. Standards Mag.*, vol. 1, no. 2, pp. 70–76, Jun. 2017.

[6] *Study on Enhancement of 3GPP Support for 5G V2X Services*, Standard 3GPP TR 22.886, V16.2.0, Nov. 2018.

[7] F. Liu, C. Masouros, A. P. Petropulu, H. Griffiths, and L. Hanzo, "Joint radar and communication design: Applications, state-of-the-art, and the road ahead," *IEEE Trans. Commun.*, vol. 68, no. 6, pp. 3834–3862, Jun. 2020.

[8] J. Wang, J. Liu, and N. Kato, "Networking and communications in autonomous driving: A survey," *IEEE Commun. Surveys Tuts.*, vol. 21, no. 2, pp. 1243–1274, 2nd Quart., 2019.

[9] N. G. Prelcic, R. M. Rial, and J. R. W. Heath, "Radar aided beam alignment in mmWave V2I communications supporting antenna diversity," in *Proc. Inf. Theory Appl.*, San Diego, CA, USA, Feb. 2016, pp. 1–7.

[10] F. Liu and C. Masouros, "A tutorial on joint radar and communication transmission for vehicular networks—Part I: Background and fundamentals," *IEEE Commun. Lett.*, vol. 25, no. 2, pp. 322–326, Feb. 2021.

[11] F. Liu and C. Masouros, "A tutorial on joint radar and communication transmission for vehicular networks—Part II: State of the art and challenges ahead," *IEEE Commun. Lett.*, vol. 25, no. 2, pp. 327–331, Feb. 2021.

[12] F. Liu and C. Masouros, "A tutorial on joint radar and communication transmission for vehicular networks—Part III: Predictive beamforming without state models," *IEEE Commun. Lett.*, vol. 25, no. 2, pp. 332–336, Feb. 2021.

[13] A. Hassanien, M. G. Amin, Y. D. Zhang, and F. Ahmad, "Signaling strategies for dual-function radar communications: An overview," *IEEE Aerosp. Electron. Syst. Mag.*, vol. 31, no. 10, pp. 36–45, Oct. 2016.

[14] P. Kumari, J. Choi, N. Gonzalez-Prelcic, and R. W. Heath, "IEEE 802.11ad-based radar: An approach to joint vehicular communication-radar system," *IEEE Trans. Veh. Technol.*, vol. 67, no. 4, pp. 3012–3027, Apr. 2018.

[15] K. Wu, J. Andrew Zhang, X. Huang, Y. Jay Guo, and R. W. Heath, "Waveform design and accurate channel estimation for frequency-hopping MIMO radar-based communications," *IEEE Trans. Commun.*, vol. 69, no. 2, pp. 1244–1258, Feb. 2021.

[16] A. R. Chiriyath, B. Paul, G. M. Jacyna, and D. W. Bliss, "Inner bounds on performance of radar and communications co-existence," *IEEE Trans. Signal Process.*, vol. 64, no. 2, pp. 464–474, Jan. 2016.

[17] Q. Zhang, Z. Li, X. Gao, and Z. Feng, "Performance evaluation of radar and communication integrated system for autonomous driving vehicles," in *Proc. IEEE INFOCOM Conf. Comput. Commun. Workshops (INFOCOM WKSHPS)*, May 2021, pp. 1–2.

[18] Q. Zhang, H. Sun, Z. Wei, and Z. Feng, "Sensing and communication integrated system for autonomous driving vehicles," in *Proc. IEEE INFOCOM Conf. Comput. Commun. Workshops (INFOCOM WKSHPS)*, Jul. 2020, pp. 1278–1279.

[19] J. A. Zhang, X. Huang, Y. J. Guo, J. Yuan, and R. W. Heath, "Multibeam for joint communication and radar sensing using steerable analog antenna arrays," *IEEE Trans. Veh. Technol.*, vol. 68, no. 1, pp. 671–685, Jan. 2019.

[20] X. Liu *et al.*, "Joint transmit beamforming for multiuser MIMO communication and MIMO radar," *IEEE Trans. Signal Process.*, vol. 55, no. 3, pp. 1213–1226, Jun. 2019.

[21] P. Kumari, S. A. Vorobyov, and R. W. Heath, "Adaptive virtual waveform design for millimeter-wave joint communication–radar," *IEEE Trans. Signal Process.*, vol. 68, pp. 715–730, 2020.

[22] Y. Liu, G. Liao, J. Xu, Z. Yang, and Y. Zhang, "Adaptive OFDM integrated radar and communications waveform design based on information theory," *IEEE Commun. Lett.*, vol. 21, no. 10, pp. 2174–2177, Oct. 2017.

[23] C. Aydogdu, M. F. Keskin, N. Garcia, H. Wymeersch, and D. W. Bliss, "RadChat: Spectrum sharing for automotive radar interference mitigation," *IEEE Trans. Intell. Transp. Syst.*, vol. 22, no. 1, pp. 416–429, Jan. 2021.

[24] F. Liu, C. Masouros, A. Li, T. Ratnarajah, and J. Zhou, "MIMO radar and cellular coexistence: A power-efficient approach enabled by interference exploitation," *IEEE Trans. Signal Process.*, vol. 66, no. 14, pp. 3681–3695, Jul. 2018.

[25] J. Qian, M. Lops, L. Zheng, X. Wang, and Z. He, "Joint system design for coexistence of MIMO radar and MIMO communication," *IEEE Trans. Signal Process.*, vol. 66, no. 13, pp. 3504–3519, Jul. 2018.

[26] Z. Cheng, B. Liao, S. Shi, Z. He, and J. Li, "Co-design for overlaid MIMO radar and downlink MISO communication systems via Cramér–Rao bound minimization," *IEEE Trans. Signal Process.*, vol. 67, no. 24, pp. 6227–6240, Dec. 2019.

[27] B. Li and A. P. Petropulu, "Joint transmit designs for coexistence of MIMO wireless communications and sparse sensing radars in clutter," *IEEE Trans. Aerosp. Electron. Syst.*, vol. 53, no. 6, pp. 2846–2864, Dec. 2017.

[28] X. Zhang, M. Peng, S. Yan, and Y. Sun, "Deep-reinforcement-learning-based mode selection and resource allocation for cellular V2X communications," *IEEE Internet Things J.*, vol. 7, no. 7, pp. 6380–6391, Jul. 2020.

[29] M. Marjanovic, A. Antonic, and I. P. Žarko, "Edge computing architecture for mobile crowdsensing," *IEEE Access*, vol. 6, pp. 10662–10674, 2018.

[30] Z. Zhang, S. Wang, Y. Hong, L. Zhou, and Q. Hao, "Distributed dynamic map fusion via federated learning for intelligent networked vehicles," 2021, *arXiv:2103.03786*.

[31] *Annex 24 to Working Party 5A Chairman's Report on Working Document Towards a Preliminary Draft New Report ITU-R M. [CAV] Connected Automated Vehicles (CAV)*, International Telecommunication Union, Geneva, Switzerland, May 2021. [Online]. Available: https://www.itu.int/dms_pub/itu-r/md/19/wp5a/c/R19-WP5A-C-0359!N24!MSW-E.docx

[32] *Technical Specification Group Services and System Aspects; Study on Enhancement of 3GPP Support for 5G V2X Services*, Standard 3GPP TR 22.886, V16.2.0, Rel. 16, Nov. 2018.

[33] F. P. Müller, "Survey on ranging sensors and cooperative techniques for relative positioning of vehicles," *Sensors*, vol. 17, no. 271, pp. 1–27, Feb. 2017.

[34] Y. Liu *et al.*, "Deep reinforcement learning for offloading and resource allocation in vehicle edge computing and networks," *IEEE Trans. Veh. Technol.*, vol. 68, no. 11, pp. 11158–11168, Nov. 2019.

[35] *Technical Specification Group Radio Access Network; NR; Physical Channels and Modulation*, Standard 3GPP TR 38.211, V16.7.0, Rel. 16, Sep. 2021.

[36] Z. Fang, Z. Wei, X. Chen, H. Wu, and Z. Feng, "Stochastic geometry for automotive radar interference with RCS characteristics," *IEEE Wireless Commun. Lett.*, vol. 9, no. 11, pp. 1817–1820, Nov. 2020.

[37] Q. Zhang, X. Wang, Z. Li, and Z. Wei, "Design and performance evaluation of joint sensing and communication integrated system for 5G mmWave enabled CAVs," *IEEE J. Sel. Topics Signal Process.*, vol. 15, no. 6, pp. 1500–1514, Nov. 2021.

[38] C. Shi, F. Wang, M. Sellathurai, and J. Zhou, "Non-cooperative game theoretic power allocation strategy for distributed multiple-radar architecture in a spectrum sharing environment," *IEEE Access*, vol. 6, pp. 17787–17800, 2018.

[39] S. Baek, I. Lee, and C. Song, "A new data pilot-aided channel estimation scheme for fast time-varying channels in IEEE 802.11p systems," *IEEE Trans. Veh. Technol.*, vol. 68, no. 5, pp. 5169–5172, May 2019.
[40] M. M. Awad, K. G. Seddik, and A. Elezabi, "Channel estimation and tracking algorithms for harsh vehicle to vehicle environments," in *Proc. IEEE 82nd Veh. Technol. Conf. (VTC-Fall)*, Sep. 2015, pp. 1–5.
[41] H. Fazlollahtabar and H. Gholizadeh, "Economic analysis of the M/M/1/N queuing system cost model in a vague environment," *Int. J. FUZZY Log. Intell. Syst.*, vol. 19, no. 3, pp. 192–203, Sep. 2019.
[42] J. Sztrik, *Basic Queuing Theory*. Debrecen, Hungary: Univ. Debrecen: Faculty of Informatics, Nov. 2012.
[43] A. Ali, N. González-Prelcic, R. W. Heath, Jr., and A. Ghosh, "Leveraging sensing at the infrastructure for mmWave communication," 2019, *arXiv:1911.09796*.
[44] M. Costa, M. Codreanu, and A. Ephremides, "Age of information with packet management," in *Proc. IEEE ISIT*, Jun. 2014, pp. 1583–1587.
[45] M. Costa, M. Codreanu, and A. Ephremides, "On the age of information in status update systems with packet management," *IEEE Trans. Inf. Theory*, vol. 62, no. 4, pp. 1583–1587, Apr. 2016.
[46] S. Sun, G. R. MacCartney, Jr., and T. S. Rappaport, "Millimeter-wave distance-dependent large-scale propagation measurements and path loss models for outdoor and indoor 5G systems," in *Proc. 10th Eur. Conf. Antennas Propag. (EuCAP)*, Davos, Switzerland, Apr. 2016, pp. 1–5.
[47] *Technical Specification Group Radio Access Network; New Frequency Range for NR*, Standard 3GPP TR 38.815, (24.25-29.5 GHz), V15.0.0, Jun. 2018.
[48] *Study on Supporting NR From 52.6 GHz to 71 GHz*, Standard 3GPP TR 38.808, V17.0.0, Rel. 17, Mar. 2021.
[49] *Working Document towards a Preliminary Draft New Report ITU-R M.[CAV] Connected Automated Vehicles (CAV)*, document ITU-R WP5A Document 5A/TEMP/171-E, Nov. 2021.

Qixun Zhang (Member, IEEE) received the B.Eng. degree in communication engineering and the Ph.D. degree in circuit and system from the Beijing University of Posts and Telecommunications (BUPT), Beijing, China, in 2006 and 2011, respectively. From March to June 2006, he was a Visiting Scholar at the University of Maryland, College Park, MD, USA. From November 2018 to November 2019, he was a Visiting Scholar with the Department of Electrical and Computer Engineering, University of Houston, Houston, TX, USA. He is currently a Professor with the Key Laboratory of Universal Wireless Communications, Ministry of Education, and the School of Information and Communication Engineering, BUPT. He is active in ITU-R WP5A/5C/5D standards. His research interests include B5G/6G mobile communication system, joint communication and sensing system for autonomous driving vehicle, mmWave communication systems, cognitive radio and heterogeneous networks, game theory, and unmanned aerial vehicles (UAVs) communication.

Hongzhuo Sun (Member, IEEE) is currently pursuing the master's degree with the School of Information and Communication Engineering, Beijing University of Posts and Telecommunications (BUPT), Beijing, China. His research interests include time-division based on joint communication and sensing system design and performance analysis.

Xinye Gao (Graduate Student Member, IEEE) is currently pursuing the master's degree with the School of Information and Communication Engineering in Beijing University of Posts and Telecommunications (BUPT), Beijing, China. His research interests include hardware testbed design for joint communication and sensing systems.

Xinna Wang (Member, IEEE) received the master's degree from the School of Information and Communication Engineering, Beijing University of Posts and Telecommunications (BUPT), Beijing, China, in 2021. Her research interests include joint communication and sensing system design for autonomous driving vehicle and game theory.

Zhiyong Feng (Senior Member, IEEE) received the B.S., M.S., and Ph.D. degrees from the Beijing University of Posts and Telecommunications (BUPT), Beijing, China. She is currently a Professor with the School of Information and Communication Engineering, BUPT, and the Director of the Key Laboratory of Universal Wireless Communications, Ministry of Education, China. She is active in standards development, such as ITU-R WP5A/5C/5D, IEEE 1900, ETSI, and CCSA. Her research interests include joint communication and sensing system design, wireless network architecture design and radio resource management, spectrum sensing and dynamic spectrum management in cognitive wireless networks, universal signal detection and identification, and network information theory.